Crystal Structures of Pyruvate Phosphate Dikinase from Maize Revealed an Alternative Conformation in the Swiveling-Domain Motion[†,‡]

Tsugumi Nakanishi,[§,||] Toru Nakatsu,[§,⊥] Makoto Matsuoka,[@] Kanzo Sakata,[||] and Hiroaki Kato*[,§,⊥]

Kinetic Crystallography Research Team, Membrane Dynamics Research Group, RIKEN Harima Institute at SPring-8, 1-1-1 Kouto, Mikazuki-cho, Sayo-gun, Hyogo 679-5148, Japan, Department of Structural Biology, Graduate School of Pharmaceutical Sciences, Kyoto University, 46-29 Yoshida-Shimo-Adachi, Kyoto 606-8501, Japan, Institute for Chemical Research, Kyoto University, Gokasyo, Uji, Kyoto 611-0011, Japan, and BioScience Center, Nagoya University, Nagoya, Aichi 464-8601, Japan

Received July 20, 2004; Revised Manuscript Received October 23, 2004

ABSTRACT: Pyruvate phosphate dikinase (PPDK) reversibly catalyzes the conversion of ATP, phosphate, and pyruvate into AMP, pyrophosphate, and phosphoenolpyruvate (PEP), respectively. Since the nucleotide binding site (in the N-terminal domain) and the pyruvate/PEP binding site (in the C-terminal domain) are separated by ∼45 Å, it has been proposed that an intermediary domain, called the central domain, swivels between these remote domains to transfer the phosphate. However, no direct structural evidence for the swiveling central domain has been found. In this study, the crystal structures of maize PPDK with and without PEP have been determined at 2.3 Å resolution. These structures revealed that the central domain is located near the pyruvate/PEP binding C-terminal domain, in contrast to the PPDK from *Clostridium symbiosum*, wherein the central domain is located near the nucleotide-binding N-terminal domain. Structural comparisons between the maize and *C. symbiosum* PPDKs demonstrated that the swiveling motion of the central domain consists of a rotation of at least 92° and a translation of 0.5 Å. By comparing the maize PPDK structures with and without PEP, we have elucidated the mode of binding of PEP to the C-terminal domain and the induced conformational changes in the central domain.

Pyruvate phosphate dikinase (PPDK,[1] ATP:pyruvate, orthophosphate phosphotransferase, EC 2.7.9.1) catalyzes the reversible conversion of ATP, P_i, and pyruvate into AMP, PP_i, and PEP, respectively, by three Mg^{2+}-dependent partial reactions that involve pyrophospho- and phosphoenzyme intermediates (*1*−*3*):

$$\text{E}-\text{His} + \text{ATP} \rightarrow \text{E}-\text{His}-\text{PP} + \text{AMP} \quad (1)$$

$$\text{E}-\text{His}-\text{PP} + \text{P}_\text{i} \rightarrow \text{E}-\text{His}-\text{P} + \text{PP}_\text{i} \quad (2)$$

$$\text{E}-\text{His}-\text{P} + \text{pyruvate} \rightarrow \text{E}-\text{His} + \text{PEP} \quad (3)$$

Each reaction is reversible, but the outcome depends on the host organism: PEP formation is physiologically favored in C_4 photosynthesis in C_4 and Crassulacean acid metabolism plants, while ATP formation is favored during glycolysis in some microorganisms (*2*). Enzymatic pyrophosphorylation (reaction 1) and phosphorylation (reaction 2) involve a histidine residue, His458, in the sequence of maize PPDK (ZmPPDK) (*4*, *5*). The nucleotide binding site is located in the N-terminal portion of the polypeptide chain, while the pyruvate/PEP binding site is located near the C-terminal region (*6*−*9*). Previous kinetic studies on the plant and bacterial PPDK mechanisms have suggested that both types of PPDK engaged an active site histidine to mediate the phosphoryl transfer, but they appeared to utilize different reaction steps (*2*). Specifically, the bacterial PPDK uses a three-step mechanism, while sugarcane and maize PPDKs employ a two-step mechanism. This finding poses the question of whether the catalytic pathways of both enzymes are the same and whether the lifetimes of the pyrophosphoryl intermediates differ between these mechanisms.

The crystal structures of the PPDKs from the bacterium *Clostridium symbiosum* [CsPPDK (*10*)] and the protozoan parasite *Trypanosoma brucei* [TbPPDK (*11*)] have recently been solved at 1.94 and 3.0 Å resolution, respectively. The PPDK structures revealed two remote substrate binding sites: an N-terminal nucleotide binding site and a C-terminal pyruvate/PEP binding site. The two binding sites are 45 Å from each other, in separate structural domains. The N-terminal domain contains 240 residues that adopt a fold termed the ATP grasp (*12*, *13*). The C-terminal pyruvate/PEP binding domain consists of 340 residues and adopts a TIM barrel motif (*14*). A third domain, called the central domain, contains the phosphate group acceptor/donor residue, which

[†] This work was partially supported by a Grant-in-Aid for Scientific Research from the Ministry of Education, Science, Sports, and Culture of Japan and by the Nagase Science and Technology Foundation. T. Nakanishi is a Junior Research Associate of RIKEN.

[‡] Coordinates and observed structure factor amplitudes for the structure described in this paper have been deposited in the Protein Data Bank (entries 1VBG and 1VBH).

* To whom correspondence should be addressed. Telephone: +81-75-753-4617. Fax: +81-75-753-9272. E-mail: katohiro@pharm.kyoto-u.ac.jp.

[§] RIKEN Harima Institute at SPring-8.

[||] Institute for Chemical Research, Kyoto University.

[⊥] Graduate School of Pharmaceutical Sciences, Kyoto University.

[@] Nagoya University.

[1] Abbreviations: PPDK, pyruvate phosphate dikinase; ATP, adenosine 5′-triphosphate; AMP, adenosine 5′-monophosphate; P_i, inorganic orthophosphate; PP_i, inorganic pyrophosphate; PEP, phosphoenolpyruvate; ZmPPDK, maize (*Zea mays*) PPDK; CsPPDK, *Clostridium symbiosum* PPDK; TbPPDK, *Trypanosoma brucei* PPDK; apo-ZmPPDK, apo form of ZmPPDK; P−ZmPPDK, ZmPPDK complexed with PEP; rmsd, root-mean-square deviation.

10.1021/bi0484522 CCC: $30.25
Published on Web 12/31/2004

is His458 in ZmPPDK and His455 in CsPPDK. The locations of the nucleotide binding sites were inferred by analogy with other enzymes containing ATP grasp folds, whereas the location of the PEP/pyruvate binding site was determined crystallographically with the substrate analogue inhibitor phosphonopyruvate (*15*). The crystal structures suggested that the central phosphohistidine domain should undergo a swiveling motion to shuttle the phosphoryl group between the two remote active sites. The central domains in both the CsPPDK and TbPPDK structures, however, were close to the N-terminal domain and assumed similar conformations. Unfortunately, no crystal structure has been reported that shows the central domain adopting a different conformation. Without structural evidence, the swiveling motion remains speculative, based on only computer modeling. We therefore hoped to obtain a crystal structure of this enzyme in an alternative conformation, to define the swiveling motion of the central domain on a structural basis. Furthermore, a comparison between both conformations would provide insight into the details of the PPDK reaction mechanism.

Herein, we report the crystal structures of ZmPPDK with and without PEP. In both structures, the central phosphohistidine domain adopted an alternative conformation thought to be a rotational intermediate of the PPDK reaction. The structures provided clues to the mechanism of the central domain motion and the roles of the linker regions between the central domain and the N-terminal or C-terminal domains. These observations represent the first structural evidence for the swiveling-domain movement of PPDK. In addition, the structure of the PEP complex showed the binding mode of the actual substrate. The complex structures provided evidence for a conformational change in the central domain upon PEP binding, even though the binding site is distant from the central domain itself.

EXPERIMENTAL PROCEDURES

Crystallization and X-ray Data Collection. ZmPPDK was purified as previously described (*16*). Crystals of ZmPPDK were grown at 25 °C by vapor diffusion in a hanging drop containing equal volumes of the PPDK solution and a reservoir solution, which consisted of 0.1 M MES (pH 6.5), 12−13% (w/v) PEG 8000, 0.1 M $MgSO_4$, and 10% glycerol. The crystals belong to monoclinic space group *C*2 with the following unit cell dimensions: $a = 108.2$ Å, $b = 100.2$ Å, $c = 108.4$ Å, and $\beta = 96.5°$. There is one monomer in the asymmetric unit, and the solvent content is 60 vol %. The average crystal dimensions were 0.3 mm × 0.4 mm × 0.05 mm.

X-ray diffraction data were collected at 100 K on beamline BL44B2 at SPring-8 using a Mar 165 charge-coupled device system (marCCD165) with a crystal−detector distance of 170 mm. The data were processed with Crystal Clear software (*17*). The details of the data processing are summarized in Table 1.

Determination of Structure by Molecular Replacement. The 2.3 Å resolution structure of CsPPDK [sequence 54% identical with that of maize PPDK, Protein Data Bank entry 1DIK (*10*)] was used as a search model for molecular replacement. Rotation and translation searches were carried out with CNS (*18*). Initial attempts to use the complete CsPPDK monomer as a search model were unsuccessful; therefore, the PPDK model was split into three domains (amino acid residues 2−340, 390−504, and 534−876) for further molecular replacement searches. The subsequent calculations performed using the C-terminal domain (334 residues with a TIM barrel topology) provided a single solution with a Patterson correlation coefficient well above the next peak (ca. 23.4% higher peak height than the second peak). The cross-validation residual R_{free} value of 0.48 is well below that expected for a random solution (ca. 0.6). The quality of the initial electron density distribution and the convergence of the refinement process of this partially (38%) complete model provided confidence that we could proceed with molecular replacement phasing.

Table 1: Diffraction Data Statistics

	apo-ZmPPDK	P−ZmPPDK
wavelength (Å)	1.00	1.02
space group	*C*2	*C*2
cell parameters		
a (Å)	108.2	109.3
b (Å)	100.2	100.5
c (Å)	108.4	108.2
β (deg)	96.5	98.5
resolution range (Å)	73.3−2.3	45.6−2.3
no. of observations	390753	207793
no. of unique reflections	51096	51391
redundancy	7.6	4.0
R_{merge} (%)[a,b]	5.4 (30.1)	7.5 (25.5)
completeness (%)[a]	100 (100)	99.9 (99.0)
$I/\sigma(I)$[a]	11.5 (2.6)	7.5 (2.5)

[a] The last shell value is in parentheses. The resolution range of the outer shells is 2.44−2.30 Å for both apo-ZmPPDK and P−ZmPPDK. [b] $R_{merge} = \sum_{hkl}|I - \langle I\rangle|/\sum_{hkl}I$.

Model Building and Refinement. Model building and refinement were carried out with TURBO-FRODO (*19*) and CNS, respectively. Initially, a model of only the C-terminal domain was rebuilt, using both the $2F_o - F_c$ and $F_o - F_c$ difference electron density maps. At an *R*-factor of 0.43, electron densities appeared that corresponded to the central domain region, and further rounds of model rebuilding and refinement were performed. At an *R*-factor of 0.38, densities corresponding to the N-terminal domain appeared and additional rounds of model construction and refinement were carried out. The final apo-ZmPPDK structural model includes 874 residues of the 876 total amino acids in the protein, one Mg^{2+} ion, three sulfate ions, and 248 water molecules. The conventional *R*-factor is 0.209, and R_{free} is 0.237, calculated using 5% of the reflections that were selected and omitted from refinement (*20*). The quality of the structural models was analyzed with PROCHECK (*21*). The refinement statistics are summarized in Table 2.

Preparation of the Ligand Complex. The PEP complex crystals were obtained by soaking the native crystals for 4 days in a solution containing 2 mM PEP, 0.1 M MES (pH 6.5), 15% (w/v) PEG 8000, 0.1 M $MgSO_4$, and 10% (v/v) glycerol. X-ray diffraction data for the complex were also collected on beamline BL45XU-PX at SPring-8. These data were processed and reduced in the same manner as the native data. The soaked crystals were isomorphous with the native crystals. The initial phases were derived from the structural model of apo-ZmPPDK, and the model rebuilding and refinement were performed in the same manner that was used for the native structure (Table 2). Stereochemical parameters

Table 2: Refinement Statistics

	apo-ZmPPDK	P−ZmPPDK
resolution range (Å)	46.0−2.3	45.6−2.3
R factor (%)[a]	20.9	23.0
no. of reflections used	50976	50481
R_{free} (%)[a]	23.7	25.9
no. of reflections used	2545	2528
no. of protein residues	874	862
no. of solvent molecules	248	194
no. of Mg^{2+} ions	1	1
no. of SO_4^{2-} ions	3	1
no. of PEP molecules	−	1
average *B* (Å^2)	39.3	52.6
rmsd for bond lengths (Å)[b]	0.009	0.008
rmsd for bond angles (deg)[b]	1.3	1.2

[a] *R*-factor $= \sum|F_o - F_c|/\sum F_o$, where F_o and F_c are the observed and calculated structure factor amplitudes, respectively. R_{free} was calculated from random selections of the reflections constituting ~5% of the total reflections, which were not used in refinement. [b] Root-mean-square deviation from ideal geometry.

of the PEP and Mg^{2+} structures derived from the HIC-Up database (*22*) were used for the refinement. The model of PEP-complexed ZmPPDK (P−ZmPPDK) includes 862 of the 876 total amino acids, PEP, Mg^{2+}, two sulfate ions, and 194 water molecules with an *R*-factor of 0.230 (R_{free} = 0.259). It is noted that the region between Arg452 and Gly454, near the active residue His458 in the central domain, was disordered.

Domain Analysis. The domain movements of PPDK were analyzed with DynDom (*23*). DynDom detects clusters of rotation vectors corresponding to main chain segments, which form dynamic domains. A dynamic domain may be composed of several regions moving in a concerted fashion without necessarily constituting a globular unit. Furthermore, a comparison of the torsion angles between the dynamic domains predicts the residues involved in rotation. Although alternate states in a protein are usually compared, in this paper, the alternate states of different proteins (ZmPPDK and CsPPDK) were compared. Since the structures of each domain between ZmPPDK and CsPPDK are similar, the structures of ZmPPDK and CsPPDK deal with those in the same protein.

Coordinates. The coordinates have been deposited in the RCSB Protein Data Bank (entries 1VBG and 1VBH).

RESULTS AND DISCUSSION

Overall Structure of ZmPPDK. ZmPPDK with or without PEP forms a homodimer, and the monomer's structure is elongated, analogous to those of the other PPDKs (*10*, *11*), with three independently folded domains (Figure 1). The monomer has overall dimensions of ca. 55 Å × 65 Å × 105 Å. The crystal belongs to space group *C*2, with a 2-fold axis parallel to the β-axis. The two PPDK monomers form an elongated dimer related to this 2-fold axis in a manner similar to that of other PPDKs.

Amino-terminal residues (3−343) form the N-terminal domain, which can be divided into three subdomains: (i) sheet 1 (residues 3−117, 200−244, and 282−286), which includes a five-stranded antiparallel β-sheet, (ii) a four-helix bundle subdomain (residues 118−199) inserted in the sheet 1 subdomain, and (iii) sheet 2 (residues 245−281 and 287−344), which also includes a five-stranded antiparallel β-sheet. The main body of the N-terminal domain adopts a typical ATP grasp fold, as observed for other nucleotide binding proteins (*13*, *24*) and described in models of other PPDKs. A number of biochemical studies (*25*) have suggested that the nucleotide binding site resides in the N-terminal domain of CsPPDK, particularly in the wide cleft formed by the β-sheets, between these subdomains. The nucleotide binding clefts of ZmPPDK and TbPPDK (*11*) are similar to and wider than that of CsPPDK (*10*), though the fold of each subdomain is nearly identical in these three PPDK structures.

The central domain (residues 394−514) represents the phosphohistidine "swiveling" domain, with residue His458 functioning to shuttle the bound phosphate group between the nucleotide binding site on the N-terminal domain and the pyruvate/PEP binding site on the C-terminal domain. This domain has an α/β-sandwich topology composed of two β-layers and one layer of α-helices. Remarkably, the central domain of ZmPPDK lies close to the C-terminal domain (Figure 1B), in contrast to the crystal structures of other PPDKs in which the central domain lies near the N-terminal domain (Figure 1C). Catalytic residue His458 of ZmPPDK (denoted with an arrow in Figure 1B) is also located near the C-terminal domain, whereas His455, the corresponding residue in CsPPDK, faces the opposite side and is buried in the N-terminal domain (the arrow in Figure 1C). Consequently, the central domain of ZmPPDK must rotate around the axis indicated in Figure 1B (see below).

The C-terminal domain (residues 536−876) is the pyruvate/PEP binding domain, consisting of a TIM barrel with three inserted regions (Glu566−Thr587, Leu622−Ser678, and Thr772−Gly812). This topology is identical to that observed for CsPPDK and TbPPDK. The pyruvate/PEP binding domain of pyruvate kinase also forms a TIM barrel with an inserted domain, called the B domain, which is known to be mobile. One of the subdomain loops (Leu622−Ser678) in ZmPPDK corresponds to the B domain of pyruvate kinase (*26*). We could clearly observe the bound PEP in the P−ZmPPDK structure. The binding site is located at the C-terminal end of the β-strands that form the complex inside the barrel. The binding site is similar to that predicted from the structure of CsPPDK complexed with phosphonopyruvate, a PEP analogue (*15*).

Two polypeptide segments connect the central domain to the N-terminal and C-terminal domains [linker-N (residues 344−393) and linker-C (residues 515−535) highlighted in pink and red, respectively, in Figures 1 and 2]. Linker-N forms a helix (LN-H1)−turn−helix (LN-H2) motif and a loop (LN-loop). LN-H1 and LN-H2 are arranged in an antiparallel manner with many interactions (Figure 2B). The residues in LN-loop (388−393) are close to the central domain and form a 3_{10}-helix. Linker-C forms a loop (LC-loop) and a helix (LC-H). LC-H lies across LN-H1 and LN-H2 and interacts with them rigidly. The LC-loop that appears in the electron density map possesses dual conformations (Figure 2B,C,E; see the Supporting Information).

Motion of the Central Domain. Structural comparisons between ZmPPDK and CsPPDK revealed the swiveling motion of the central domain during the catalytic reaction of PPDK. Thus, the central domain of ZmPPDK is located close to the pyruvate/PEP binding domain [the C-terminal domain (Figure 1B)], whereas that of CsPPDK is located

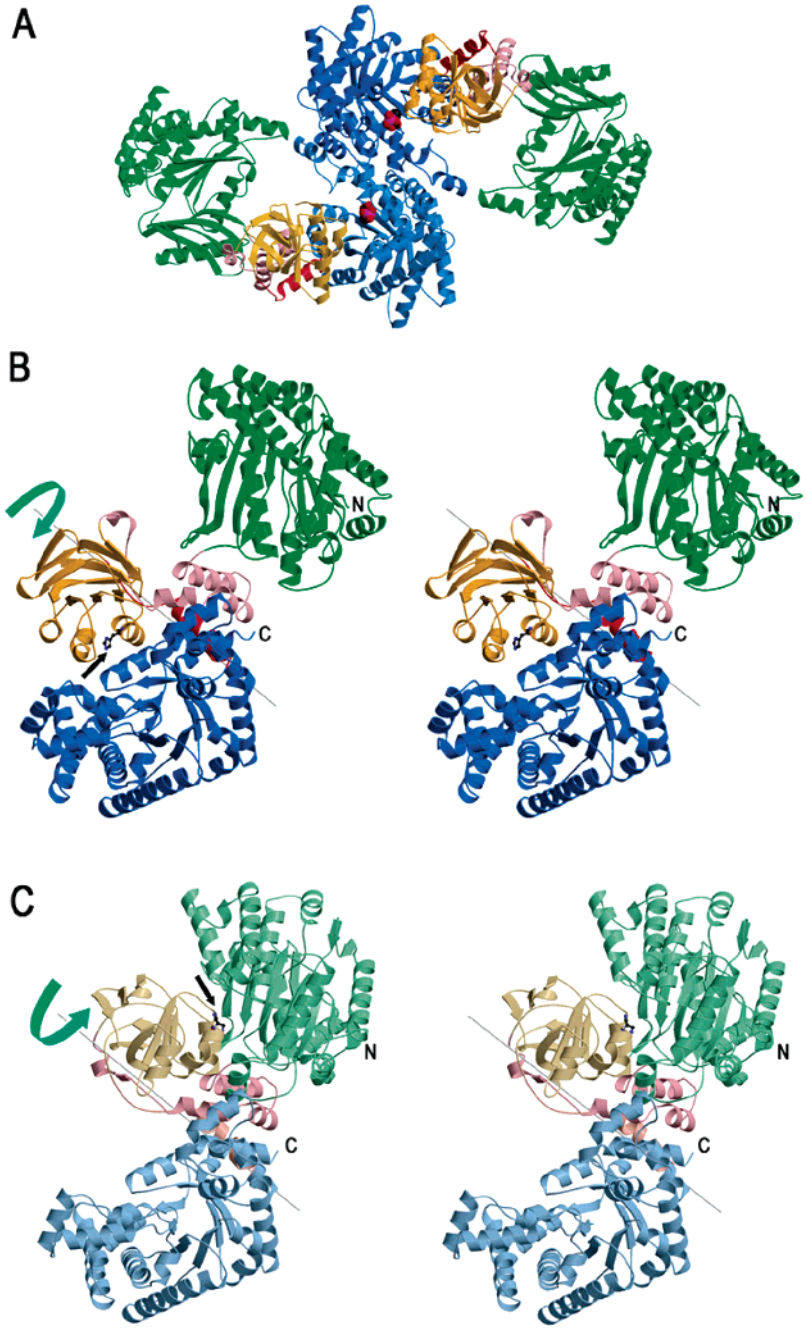

FIGURE 1: Overall structure of the ZmPPDK molecule. Structural domains are highlighted in different colors: green for the nucleotide binding domain, yellow for the central domain, blue for the pyruvate/PEP binding domain, and pink and red for linker peptides (see Figure 2). (A) Overall structure of the PEP-bound form of the ZmPPDK dimer. The PEP molecule is shown as a CPK model. (B and C) Stereoviews showing ZmPPDK and CsPPDK, respectively. The transition from ZmPPDK (B) to CsPPDK (C) must utilize a rotation of the central domain (yellow and grayish yellow) of 92.1° about the axis shown in gray. This dramatic rotation is evident from the large shifts of catalytic residue His458 in ZmPPDK and His455 in CsPPDK, shown by a ball-and-stick model (black arrow) and the polypeptide chain. Panel C was drawn using the coordinates of PPDK from *C. symbiosum* (PDB entry 1KBL). Figures 1−4 were prepared with MOLSCRIPT (*29*), SPOCK (*30*), and Raster3D (*31*).

close to the N-terminal nucleotide binding domain (Figure 1C). Using the pyruvate/PEP binding domain as a reference, the nucleotide binding domain exhibits a few differences in both the relative position and the orientation between the structures of ZmPPDK and CsPPDK. Nevertheless, the relative orientation of the N-terminal subdomains significantly differs between the structures of ZmPPDK and CsPPDK. Furthermore, within the central domain, only small conformational changes exist between the structures of ZmPPDK and CsPPDK. These findings indicate that the central domain is moved by rotation as a rigid body, with few conformational changes within the domain. This movement is similar to that predicted by model building (*10*). An analysis of the conformational changes between ZmPPDK and CsPPDK with DynDom (*23*) showed that the central domain rotates 92.1° about the axis shown in panels B and C of Figure 1 and moves 0.5 Å closer to the pyruvate/PEP binding domain.

Linker-N and linker-C must act as the swivel, since the axis of rotation lies parallel to the linker region. To identify the parts of the linkers that contribute to the motion, each linker of ZmPPDK was superposed on top of its counterpart

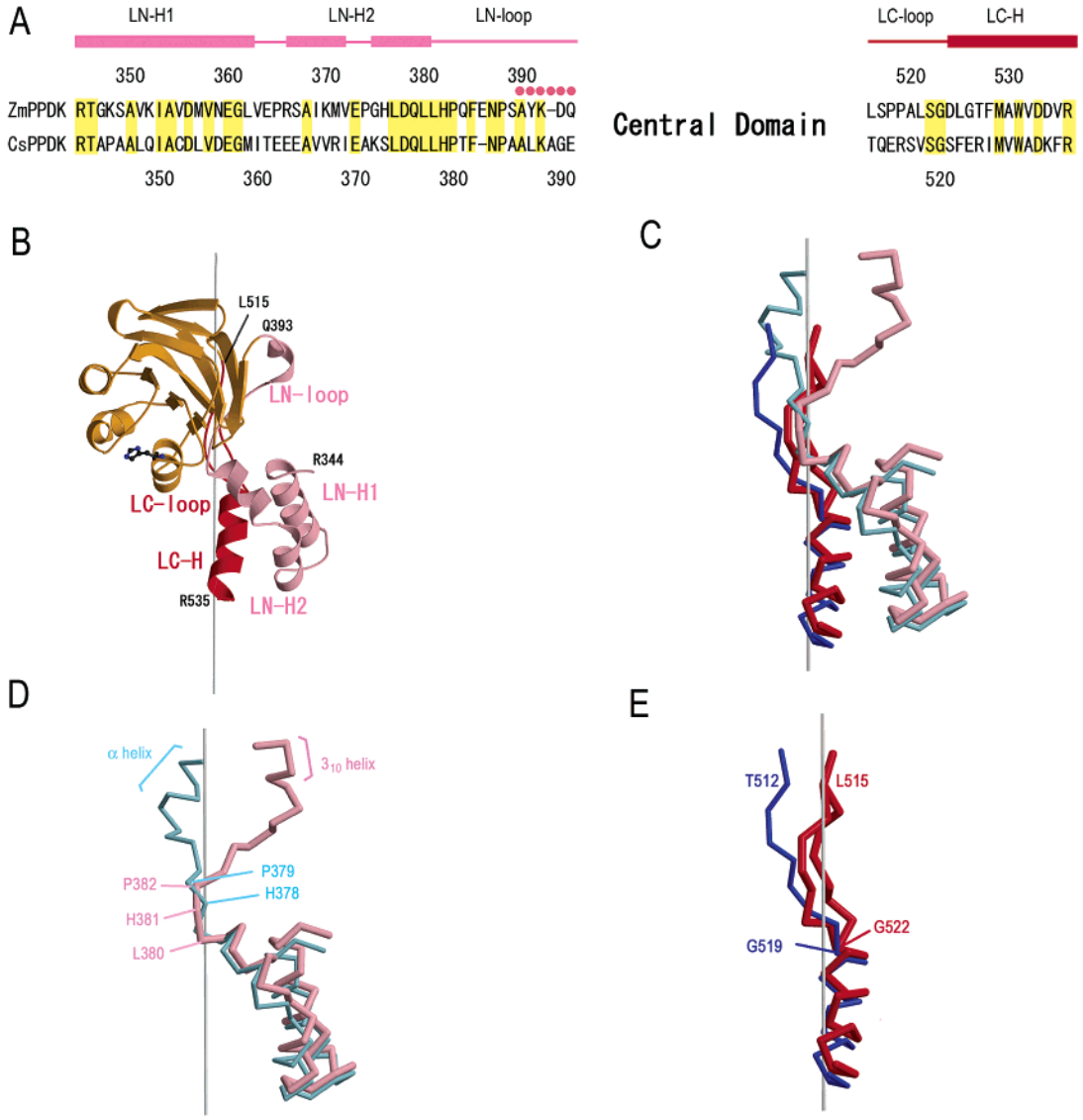

FIGURE 2: Linker region structures. (A) Sequence alignment of the ZmPPDK and CsPPDK linker regions with secondary structure elements, i.e., α-helices (rectangles) and turn and loops (lines). The conserved residues within each pair are highlighted in yellow. The residues that form the 3_{10}-helix are denoted with magenta circles above the sequences. (B) Linker region, central domain, and the axis of rotation. The linker region consists of two chains, linker-N and linker-C, which are composed of residues 344−393 and 515−535, respectively. Linker-N is divided into LN-H1, LN-H2, and LN-loop; linker-C consists of LC-H and LC-loop. LC-loop (residues 515−522) possesses dual conformations. (C) Entire linker region of ZmPPDK (pink and red) is superposed onto its counterpart in CsPPDK (light blue and blue), with both represented as C_α traces. (D) The linker-N regions of ZmPPDK (pink) and CsPPDK (light blue), depicted as C_α traces, are superposed. (E) The C_α traces of the linker-C regions of ZmPPDK (red) and CsPPDK (blue) are superposed.

in CsPPDK (Figure 2C). This superposition demonstrated that the three helices (LN-H1, LN-H2, and LC-H) were fixed, while the loops (LN-loop and LC-loop) were displaced. These findings suggest that the central domain rotates in association solely with the conformational changes of the loops, relative to the fixed helices.

The structural comparison also provides further insights into the internal motions of the loops. Linker-N of ZmPPDK is bent at the joint between LN-H2 and LN-loop (Figure 2D). The joint lies on the axis of rotation, and LN-loop becomes more displaced (between ZmPPDK and CsPPDK) on either side of the axis as the distance from the joint increases (Figure 2D). This suggests that LN-loop may kink at the joint, while the rest of the loop remains unchanged. In fact, DynDom analysis suggested that the changes in the torsion angles occur almost solely at His381 and Pro382, while those of the other residues in LN-loop are nearly unchanged. All side chains in LN-loop protrude into the solvent; thus, the loop's motion would be free from steric clashes. His381 at the hinge, however, interacts with the side chains of Asp377, which may restrict the rotation. On the other hand, linker-C lies entirely along the axis of rotation (Figure 2E). DynDom analysis shows that the torsion angle changes for linker-C are distributed over LC-loop (Leu515−Gly522). Therefore, it appears that LC-loop is flexible and the residues in LC-loop could move evenly in association with the central domain's rotation. Consequently, the swiveling of the central domain appears to be more flexible than that expected by a simple rotation at a pivot site, since the swiveling arm, especially linker-C, consists of a wide range of the residues with variable conformations.

The 3_{10}-helix in LN-loop of ZmPPDK also seems to augment the flexibility of the central domain (Figure 2D). The corresponding region of CsPPDK forms an α-helix,

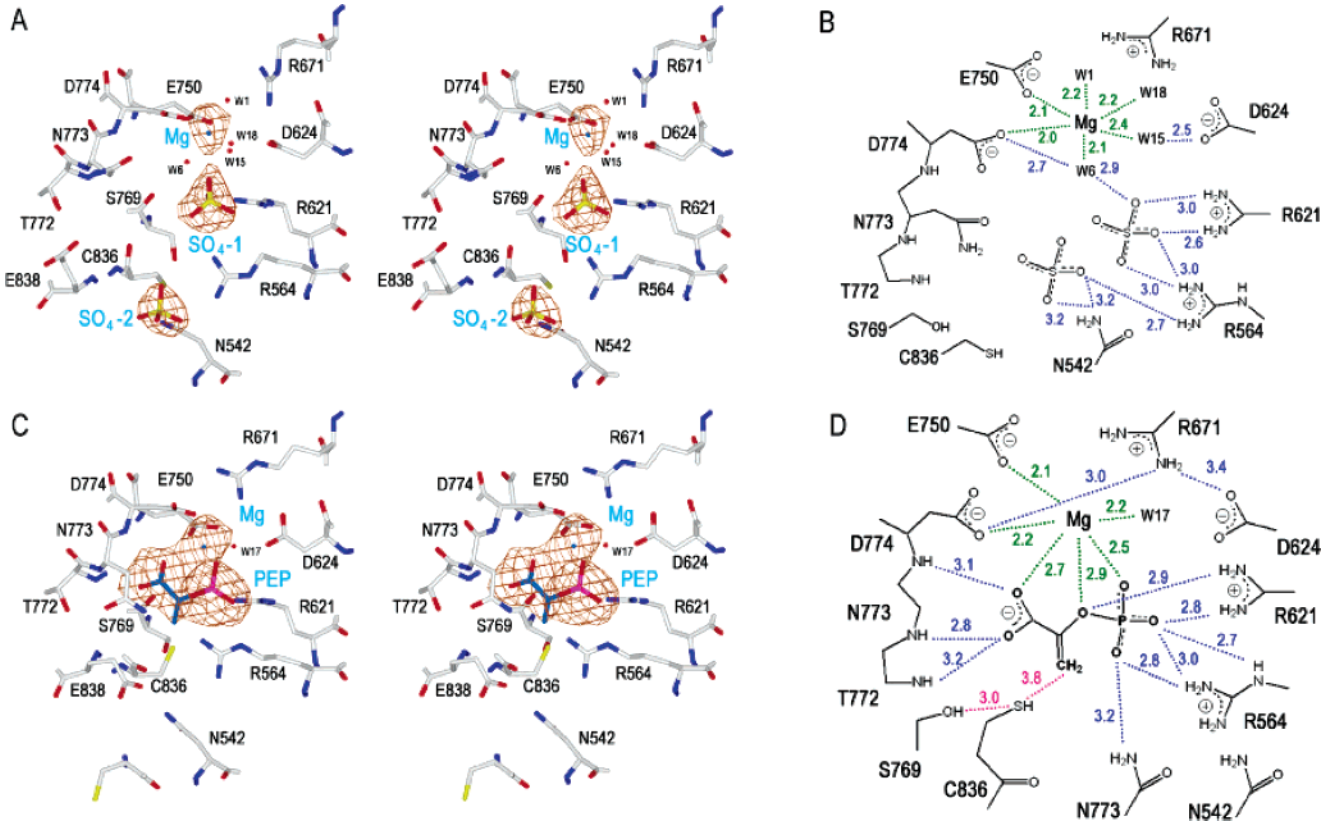

FIGURE 3: Pyruvate/PEP binding site. Stereoviews of the region surrounding the binding site in the apo form and the PEP-bound form of ZmPPDK are shown in panels A and C, respectively. Water molecules and Mg^{2+} ions are shown as red and blue spheres, respectively. The $F_o - F_c$ omit electron density map (3σ) for Mg^{2+} ion and SO_4^{2-} ions and PEP are superimposed. Schematic representations of the binding site of the apo and PEP-bound forms of ZmPPDK are shown in panels B and D, respectively. The electrostatic and polar interactions between the protein residues and the ligands are shown as blue dotted lines, except those for Mg^{2+} (green dotted lines). The interactions between the SH group of Cys836 and the atoms that participate in protonation or attacks are shown as pink dotted lines.

whereas that of TbPPDK forms a helical loop. Thus, each helical structure has a different pitch. Wei *et al*. (*27*) reported that the CsPPDK activity was not impaired even when three residues were deleted from the region corresponding to the 3_{10}-helix of ZmPPDK. Thus, this helix region is likely to be flexible enough to avoid steric distortion during the motion of central domain swiveling.

In this structure of ZmPPDK complexed with PEP, the catalytic His458 residue is located rather distant (~14 Å between the NE2 atom of His458 and the phosphorus atom of PEP) from the pyruvate/PEP binding site. The distance must be approximately 3 Å for an actual reaction to occur, and the swivel movement described above is not sufficient for the catalytic His458 to encounter the PEP. Therefore, we simulated an additional movement required for the reaction to occur by altering the torsion angles of His381, Pro382, and Ser516−Gly522 in the linker regions. This movement conforms to the swiveling mechanism we described above. However, this simulation reveals that steric clashes occur in two regions between the central domain and the C-terminal domain: between Glu415−Ala417 (of the central domain) and Phe569−Ala571 (C-terminal domain), as well as between Asp481 (central domain) and Pro632 (C-terminal domain). Thus, Glu415−Ala417 are located on the loop formed by Gln409−Ile428 in the central domain, while Phe569−Ala571 are located on an inserted region (Glu566−Thr587) of the TIM barrel in the C-terminal domain. Asp481 is located at the turn on another loop (Gly476−Gly489) in the central domain, while Pro632 is on the other inserted region (Leu622−Ser678) of the C-terminal domain. Therefore, it appears that the flexibility of the regions helps to avoid steric clashes during the catalytic reaction.

Ligand Binding Site. The structure of apo-ZmPPDK includes one Mg^{2+} and two sulfate ions near the plausible binding site for pyruvate/PEP (Figure 3A,B). The Mg^{2+} ion forms the typical octahedral coordination geometry with the side chains of Glu750 and Asp774, and with four water molecules, at distances of 2.0−2.2 Å. The sulfate ion (SO_4^-) is within hydrogen bonding distance of two amino acid residues. The distances between the O1 and O4 atoms of the sulfate ion and the NH1 atom of Arg564 are 3.0 and 2.9 Å, respectively, and the distances between the O3 and O1 atoms and the NH1 and NH2 atoms of Arg621 are 2.6 and 3.0 Å, respectively. The O2 atom interacts solely with a water molecule. The other sulfate ion, SO_4^{2-}, is located 7.3 Å from SO_4^- and interacts with the NH2 atom of Arg564 and the ND2 atom of Asn542.

In the structure of P−ZmPPDK, the sulfate ion, SO_4^-, in apo-ZmPPDK is replaced with a PEP molecule, and lacks the electron densities provided by SO_4^{2-} (Figure 3C,D). The bound PEP interacts with Arg564, Arg621, Thr772, Asn773, and Asp774. These residues are strictly conserved in other PPDKs. It has been proposed that Cys836 might participate in the enolization of pyruvate as a proton donor and/or acceptor (*28*). In apo-ZmPPDK, it adopts a single conformation in which the side chain SH points away from the PEP site, while in P−ZmPPDK, the side chain of Cys836 is located within the PEP binding site and adopts two confor-

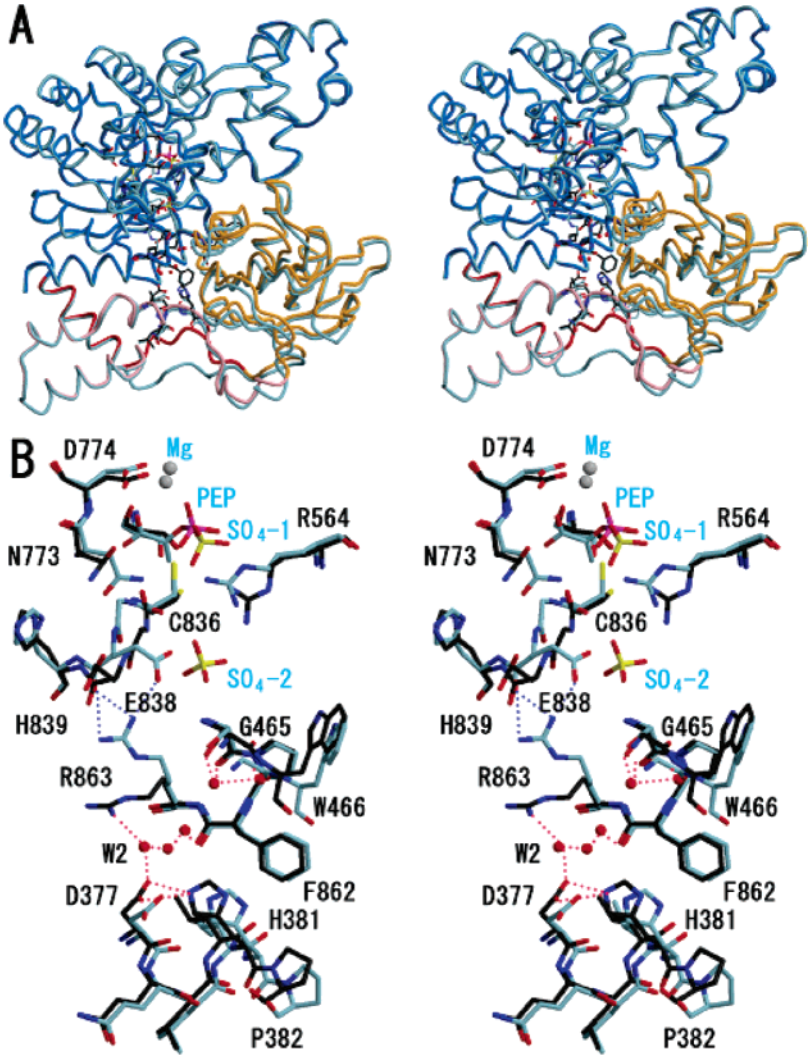

FIGURE 4: Superposition of the apo and PEP-bound forms of ZmPPDK. (A) Overall structures, without the N-terminal domain. For apo-ZmPPDK, the C-terminal domain is blue, linker-N is pink, linker-C is red, and the central domain is yellow. P−ZmPPDK is colored gray for all domains. (B) Structures around the PEP binding sites and the conformational changes of residues upon PEP binding. Apo-ZmPPDK residues are colored black and P−ZmPPDK residues gray. Oxygen atoms are colored red; the phosphorus atom is colored magenta, and sulfur atoms are colored yellow. The electrostatic and polar interactions of the residues in apo-ZmPPDK are shown as red dotted lines and those in P−ZmPPDK as blue dotted lines.

mations. In the favored conformation, the SH group is close to the methylene group of the bound PEP. In P−ZmPPDK, the SH group of Cys836 also interacts with the hydroxy group of Ser769, at a distance of 3.0 Å. The hydroxy group of Ser769 is also flipped by 87° as compared to that of apo-ZmPPDK. The carboxy group of PEP interacts with the main chain amides of Asn773 and Asp774, while the phosphate group binds the side chains of Arg564, Arg621, and Asn773. Superposition of the structures of apo-ZmPPDK and P−ZmPPDK indicates that the positions of the sulfate ion (SO_4^-) in apo-ZmPPDK and that of the phosphate group of PEP in P−ZmPPDK are slightly different. The same residues interact with the sulfate ion in apo-ZmPPDK as with the phosphate group in P−ZmPPDK. Nevertheless, due to a 1.0 Å shift of the sulfur atom relative to the phosphorus atom, the side chain conformations of Arg621 and Asn773 are altered. As in apo-ZmPPDK, a Mg^{2+} ion is also observed in P−ZmPPDK, although the octahedral coordination geometry is distorted; only three interactions with Glu750 (2.1 Å), Asp774 (2.2 Å), and a water molecule (2.2 Å) are ideal, while those with O2′ (2.7 Å), O3P (2.5 Å), and O2 (2.9 Å) of PEP are longer than the ideal length.

Conformational Changes upon PEP Binding. The central domain of ZmPPDK undergoes conformational changes that may be induced by binding of PEP to the C-terminal domain and then transmitted through linker-C (Figure 4A,B). As described above, PEP binding causes changes in the side chain conformation of Cys836 on the loop of Cys836−His839, and the entire loop also exhibits structural changes. Thus, Glu838 on the loop interacts with Arg863, while this interaction is lost in apo-ZmPPDK. Interestingly, in apo-ZmPPDK, Arg863 interacts instead with Asp377 in the linker region via the water molecule (W2). Asp377 also interacts with His381, which is at the pivot where the central domain swivels. Thus, PEP binding may cause the interacting partner of Arg863 to switch from Asp377−His381 to Glu838. The absence of an indirect interaction between Arg863 and His381 may allow His381 to move freely, breaking the interaction between the C-terminal domain and the linker region. In this manner, binding of PEP to the C-terminal

domain may serve as a trigger for the swiveling motion of the central domain.

The observed movement in the central domain induced by PEP binding would be too small to be seen actually in solution because the movement of the central domain is highly restricted by crystal packing. Indeed, residues Asp416, Gln423, and Glu495 in the central domain interact with those of Asn830 and Arg825 in the C-terminal domain of the adjacent molecule in the crystal lattice.

In conclusion, we have reported crystal structures of maize PPDK at 2.3 Å resolution. On the basis of the structures of ZmPPDK, we have demonstrated that a conformational change occurs in the central domain and have identified key residues involved in the domain swiveling motion. We also revealed the PEP binding site and the structural changes induced by PEP binding. This structural study provides the first evidence for the swiveling-domain mechanism of the PPDK reaction, which should yield insights into the mechanisms of other multidomain proteins.

ACKNOWLEDGMENT

We gratefully acknowledge the staff for assistance in the collection of X-ray data on the RIKEN beam lines at SPring-8, and the Supercomputer Laboratory at the Institute for Chemical Research, Kyoto University, for providing CPU time. We also thank Dr. Jun Hiratake of Kyoto University and Dr. Yuichiro Maéda of RIKEN for valuable discussions and critical reading of the manuscript.

SUPPORTING INFORMATION AVAILABLE

σA-weighted $2F_o - F_c$ omit electron density map (stereoview) showing the atomic arrangement of the dual loop region between Leu515 and Gly522. Contours are drawn at 0.8σ. The atomic model is drawn as a stick representation, and atoms are color-coded as follows: white for carbon, blue for nitrogen, and red for oxygen. The molecular model was prepared using SPOCK. This material is available free of charge via the Internet at http://pubs.acs.org.

REFERENCES

1. Wood, H. G., O'Brien, W. E., and Michaels, G. (1977) Properties of carboxytransphosphorylase; pyruvate, phosphate dikinase; pyrophosphate-phosphofructikinase and pyrophosphate-acetate kinase and their roles in the metabolism of inorganic pyrophosphate, *Adv. Enzymol. 45*, 85−155.
2. Carroll, L. J., Dunaway-Mariano, D., Smith, C. M., and Chollet, R. (1990) Determination of the catalytic pathway of C4-leaf pyruvate, orthophosphate dikinase from maize, *FEBS Lett. 274*, 178−180.
3. Carroll, L. J., Mehl, A. F., and Dunaway-Mariano, D. (1989) The mode of triple phosphoryl group transfer in pyruvate phosphate dikinase catalysis. Demonstration of the intermediacy of pyrophosphorylated and phosphorylated enzyme species, *J. Am. Chem. Soc. 111*, 5965−5967.
4. Pocalyko, D. J., Carroll, L. J., Martin, B. M., Babbitt, P. C., and Dunaway-Mariano, D. (1990) Analysis of sequence homologies in plant and bacterial pyruvate phosphate dikinase, enzyme I of the bacterial phosphoenolpyruvate: Sugar phosphotransferase system and other PEP-utilizing enzymes. Identification of potential catalytic and regulatory motifs, *Biochemistry 29*, 10757−10765.
5. Matsuoka, M., Ozeki, Y., Yamamoto, N., Hirano, H., Kano-Murakami, Y., and Tanaka, Y. (1988) Primary structure of maize pyruvate, orthophosphate dikinase as deduced from cDNA sequence, *J. Biol. Chem. 263*, 11080−11083.
6. McGuire, M., Carroll, L. J., Yankie, L., Thrall, S. H., Dunaway-Mariano, D., Herzberg, O., Jayaram, B., and Haley, B. H. (1996) Determination of the nucleotide binding site within *Clostridium symbiosum* pyruvate phosphate dikinase by photoaffinity labeling, site-directed mutagenesis, and structural analysis, *Biochemistry 35*, 8544−8552.
7. McGuire, M., Huang, K., Kapadia, G., Herzberg, O., and Dunaway-Mariano, D. (1998) Location of the phosphate binding site within *Clostridium symbiosum* pyruvate phosphate dikinase, *Biochemistry 37*, 13463−13474.
8. Xu, Y., McGuire, M., Dunaway-Mariano, D., and Martin, B. M. (1995) Separate site catalysis by pyruvate phosphate dikinase as revealed by deletion mutants, *Biochemistry 34*, 2195−2202.
9. Yankie, L., Xu, Y., and Dunaway-Mariano, D. (1995) Location of the catalytic site for phosphoenolpyruvate formation within the primary structure of *Clostridium symbiosum* pyruvate phosphate dikinase. 2. Site-directed mutagenesis of an essential arginine contained within an apparent P-loop, *Biochemistry 34*, 2188−2194.
10. Herzberg, O., Chen, C. C., Kapadia, G., McGuire, M., Carroll, L. J., Noh, S. J., and Dunaway-Mariano, D. (1996) Swiveling-domain mechanism for enzymatic phosphotransfer between remote reaction sites, *Proc. Natl. Acad. Sci. U.S.A. 93*, 2652−2657.
11. Cosenza, L. W., Bringaud, F., Baltz, T., and Vellieux, F. M. (2002) The 3.0 Å resolution crystal structure of glycosomal pyruvate phosphate dikinase from *Trypanosoma brucei*, *J. Mol. Biol. 318*, 1417−1432.
12. Murzin, A. G. (1996) Structural classification of proteins: New superfamilies, *Curr. Opin. Struct. Biol. 6*, 386−394.
13. Yamaguchi, H., Kato, H., Hata, Y., Nishioka, T., Kimura, A., Oda, J., and Katsube, Y. (1993) Three-dimensional structure of the glutathione synthetase from *Escherichia coli* B at 2.0 Å resolution, *J. Mol. Biol. 229*, 1083−1100.
14. Nagano, N., Orengo, C. A., and Thornton, J. M. (2002) One fold with many functions: The evolutionary relationships between TIM barrel families based on their sequences, structures and functions, *J. Mol. Biol. 321*, 741−765.
15. Herzberg, O., Chen, C. C., Liu, S., Tempczyk, A., Howard, A., Wei, M., Ye, D., and Dunaway-Mariano, D. (2002) Pyruvate site of pyruvate phosphate dikinase: Crystal structure of the enzyme-phosphonopyruvate complex, and mutant analysis, *Biochemistry 41*, 780−787.
16. Nakanishi, T., Ohki, Y., Oda, J., Matsuoka, M., Sakata, K., and Kato, H. (2004) Purification, crystallization and preliminary X-ray diffraction studies on pyruvate phosphate dikinase from maize, *Acta Crystallogr. D60*, 193−194.
17. Pflugrath, J. W. (1999) The finer things in X-ray diffraction data collection, *Acta Crystallogr. D55*, 1718−1725.
18. Brunger, A. T., Adams, P. D., Clore, G. M., DeLano, W. L., Gros, P., Grosse-Kunstleve, R. W., Jiang, J. S., Kuszewski, J., Nilges, M., Pannu, N. S., Read, R. J., Rice, L. M., Simonson, T., and Warren, G. L. (1998) Crystallography & NMR system: A new software suite for macromolecular structure determination, *Acta Crystallogr. D54*, 905−921.
19. Roussel, A., and Cambillau, C. (1989) in *Silicon graphics geometry partners directory*, pp 77−79, Silicon Graphics, Mountain View, CA.
20. Brunger, A. T. (1992) Free *R* value: A novel statistical quantity for assessing the accuracy of crystal structures, *Nature 355*, 472−475.
21. Laskowski, R. A., MacArthur, M. W., Moss, D. S., and Thornton, J. M. (1993) PROCHECK: A program to check the stereochemical quality of protein structures, *J. Appl. Crystallogr. 26*, 283−291.
22. Kleywegt, G. J., and Jones, T. A. (1998) Databases in protein crystallography, *Acta Crystallogr. D54*, 1119−1131.
23. Hayward, S., and Berendsen, H. J. (1998) Systematic analysis of domain motions in proteins from conformational change: New results on citrate synthase and T4 lysozyme, *Proteins 30*, 144−154.
24. Wolodko, W. T., Fraser, M. E., James, M. N., and Bridger, W. A. (1994) The crystal structure of succinyl-CoA synthetase from *Escherichia coli* at 2.5-Å resolution, *J. Biol. Chem. 269*, 10883−10890.
25. Ye, D., Wei, M., McGuire, M., Huang, K., Kapadia, G., Herzberg, O., Martin, B. M., and Dunaway-Mariano, D. (2001) Investigation of the catalytic site within the ATP-grasp domain of *Clostridium symbiosum* pyruvate phosphate dikinase, *J. Biol. Chem. 276*, 37630−37639.
26. Larsen, T. M., Benning, M. M., Wesenberg, G. E., Rayment, I., and Reed, G. H. (1997) Ligand-induced domain movement in

pyruvate kinase: Structure of the enzyme from rabbit muscle with Mg^{2+}, K^+, and L-phospholactate at 2.7 Å resolution, *Arch. Biochem. Biophys. 345*, 199−206.

27. Wei, M., Ye, D., and Dunaway-Mariano, D. (2001) Investigation of the role of the domain linkers in separate site catalysis by *Clostridium symbiosum* pyruvate phosphate dikinase, *Biochemistry 40*, 13466−13473.
28. Xu, Y., Yankie, L., Shen, L., Jung, Y. S., Mariano, P. S., Dunaway-Mariano, D., and Martin, B. M. (1995) Location of the catalytic site for phosphoenolpyruvate formation within the primary structure of *Clostridium symbiosum* pyruvate phosphate dikinase. 1. Identification of an essential cysteine by chemical modification with [1-^{14}C]bromopyruvate and site-directed mutagenesis, *Biochemistry 34*, 2181−2187.
29. Kraulis, P. J. (1991) MOLSCRIPT: A program to produce both detailed and schematic plots of protein structures, *J. Appl. Crystallogr. 24*, 946−950.
30. Christopher, B. T. (1998) SPOCK: Real-time collaborative molecular modelling, *J. Mol. Graphics Modell. 16*, 285−285.
31. Merritt, E. A., and Bacon, D. J. (1997) Raster3D: Photorealistic Molecular Graphics, *Methods Enzymol. 277*, 505−524.

BI0484522